13th World Conference on Earthquake Engineering
Vancouver, B.C., Canada
August 1-6, 2004
Paper No. 450

TRI-AXIAL MULTI-LINEAR RESTORING FORCE MODEL OF R/C STRUCTURES BY USING AN ANALOGY TO THE THEORY OF PLASTICITY

Koshiro NISHIMURA[1], Katsuki TAKIGUCHI[2] and H.H. NGUYEN[3],

SUMMARY

It is necessary to formulate tri-axial non-linear restoring force characteristics for examination of tri-axial earthquake responses of buildings. Nishimura and Takiguchi presented modeling method of the characteristics of R/C structures in 2003, which was based on the theory of plasticity. In this paper, tri-axial multi-linear restoring force models of R/C structures presented by Nishimura and Takiguchi, which were flexural type model and shear type model, were modified in evaluation of rigidity. These models were used for earthquake response analyses of one-mass-system. As a result, comparison of numerical results between tri-axial and bi-axial response analyses showed that it was enough to consider two-directional input of earthquake motion to estimate lateral external force and maximum displacement in seismic design, the maximum vertical absolute acceleration responses were obtained in the range of 300 to 1,100 cm/sec^2, and then evaluation of total energy input were carried out.

INTRODUCTION

An earthquake response analysis is one of the effective techniques to estimate seismic safety of building subjected to earthquake excitation. It is necessary to formulate restoring force characteristics of the structures for the response analysis. A modeling method used an analogy to the theory of plasticity is one of the macro modeling methods. Regarding this method, Takizawa [1] presented bi-axial model of R/C structures in 1976. Yoshimura [2] modified the model presented by Takizawa in 1985. Isozaki [3] presented tri-axial model in 1992. One of the problems of tri-axial model is how to describe axial deformation behavior, which direct to compressive side on unloading stage [4][5]. Nishimura and Takiguchi presented tri-axial modeling method in 2001 that resolved above-mentioned problem [6].

In this paper, tri-axial multi-linear restoring force models of R/C structures presented by Nishimura and Takiguchi [6], which were flexural type model and shear type model, were modified in evaluation of rigidity. The flexural type has large area in hysterisis loop, and the shear type has small area in the loop,

[1] Assistant Professor, Tokyo Institute of Technology, Japan. Email: knishimu@tm.mei.titech.ac.jp
[2] Professor, Tokyo Institute of Technology, Japan. Email: ktakiguc@tm.mei.titech.ac.jp
[3] Graduate Student, Tokyo Institute of Technology, Japan. Email: huyhoang76@tm.mei.titech.ac.jp

where the area means energy dissipation. The former one can be seen in rigid frame structures, and the later one can be seen in R/C box wall structures. These two types of one-axial restoring force characteristics were modeled in tri-linear curves, and those one-axial restoring force models were expanded to tri-axial. Tri-axial non-linear earthquake response analyses of one-mass-system were carried out with these two types of restoring force model.

RESTORING FORCE MODEL

One-axial restoring force model

Restoring force characteristics can be represented with skeleton curve and hysterisis loop. Both of flexural and shear types were modeled in tri-linear skeleton curves as shown in Figure 1. Two lateral directions and vertical direction are corresponded to X-axis, Y-axis, and Z-axis, respectively. Z-axis takes compressive side as positive direction. One-axial restoring force model of Y-axis is assumed to be equal to that of X-axis in this paper. Q_X-δ_X relationships shown in Figure 1 are expressed when N=$_C$N, which $_C$N is axial force of 0.5 axial force ratio. The models of flexural and shear types are called F-model and S-model hereinafter, respectively. First, second and third inclinations of the skeleton curve express rigidities of elastic state, cracking state, and yield state, respectively. A point beyond the maximum deformation experienced moves on the skeleton curve until unloading, and the point direct toward the point of the maximum deformation experienced after unloading, as shown in Figure 2(a). After yielding, as shown in Figure 1, loops of F-model and S-model were modeled in a parallelogram and a straight line, respectively. Condition shown in Figure 2(b) that inclination of a-b' is larger than inclination of a-b may occur. In a case like this, a rule to take a-b is applied in this model.

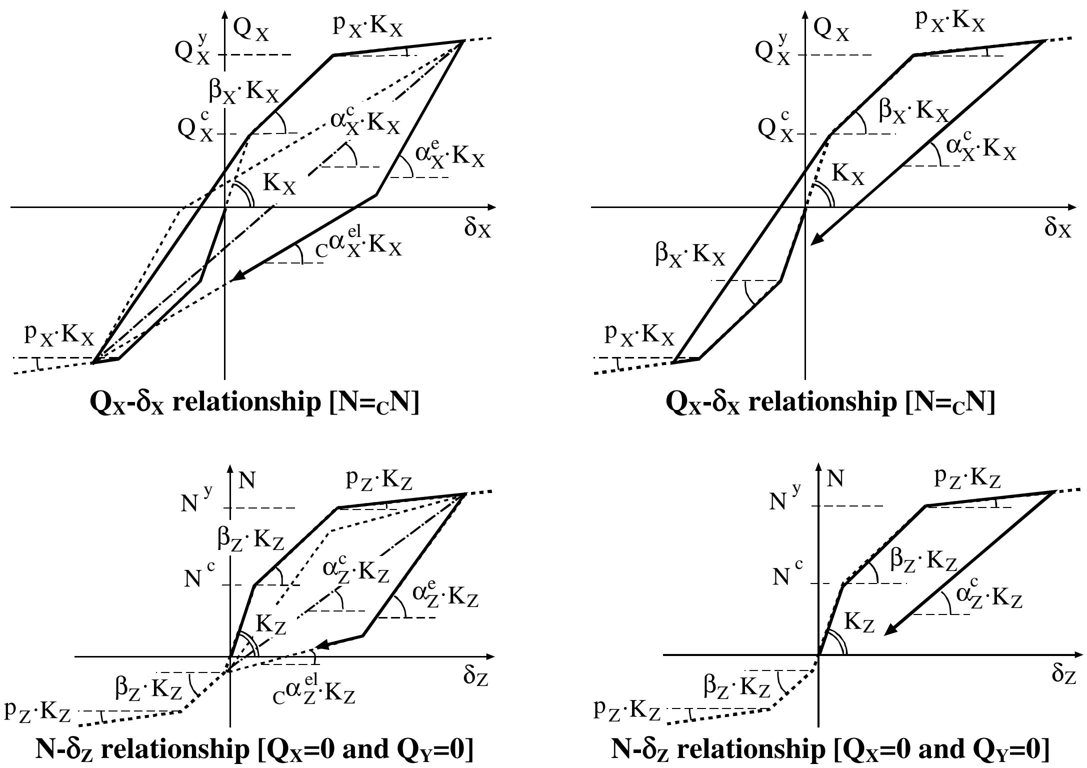

(a) F-model **(b) S-model**

Figure 1 One-axial restoring force model

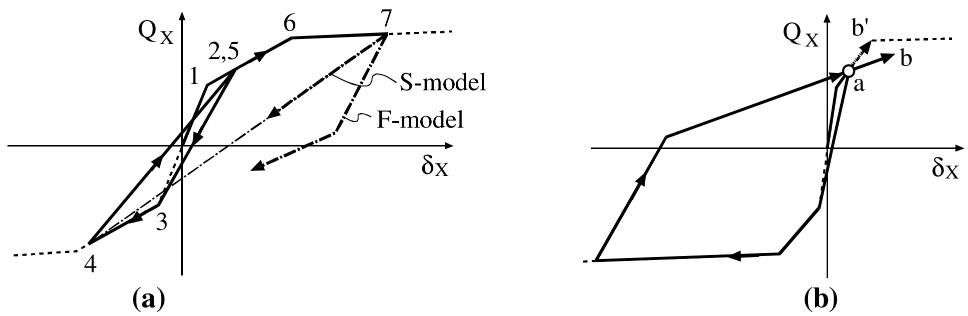

Figure 2 Rule of shift

Yield surface and cracking surface

Surfaces

Figure 3 shows cracking surface and yield surface those are corresponded to first and second corners of the skeleton curve, respectively. The F-model has parabola surfaces and the S-model has ellipse, and cracking condition and yield condition are expressed as follows.

$$F^c = \sqrt{\left(\frac{Q_X - {}_C Q_X^c}{{}_m Q_X^c}\right)^2 + \left(\frac{Q_X - {}_C Q_Y^c}{{}_m Q_Y^c}\right)^2} + \left(\frac{N - {}_C N^c}{{}_m N^c}\right)^2 - 1 \quad \text{[Cracking condition of F-model]} \tag{1}$$

$$F^y = \sqrt{\left(\frac{Q_X - {}_C Q_X^y}{{}_m Q_X^y}\right)^2 + \left(\frac{Q_X - {}_C Q_Y^y}{{}_m Q_Y^y}\right)^2} + \left(\frac{N - {}_C N^y}{{}_m N^y}\right)^2 - 1 \quad \text{[Yield condition of F-model]} \tag{2}$$

$$F^c = \left(\frac{Q_X - {}_C Q_X^c}{{}_m Q_X^c}\right)^2 + \left(\frac{Q_X - {}_C Q_Y^c}{{}_m Q_Y^c}\right)^2 + \left(\frac{N - {}_C N^c}{{}_m N^c}\right)^2 - 1 \quad \text{[Cracking condition of S-model]} \tag{3}$$

$$F^y = \left(\frac{Q_X - {}_C Q_X^y}{{}_m Q_X^y}\right)^2 + \left(\frac{Q_X - {}_C Q_Y^y}{{}_m Q_Y^y}\right)^2 + \left(\frac{N - {}_C N^y}{{}_m N^y}\right)^2 - 1 \quad \text{[Yield condition of S-model]} \tag{4}$$

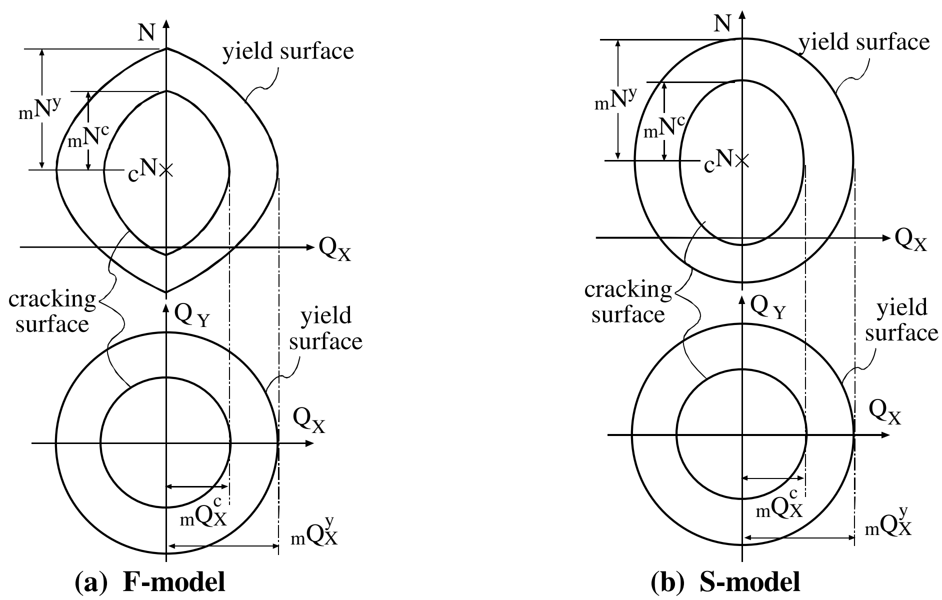

Figure 3 Cracking surface and yield surface

A force point and a deformation point are expressed as $\{P\}=(Q_X, Q_Y, N)^T$ and $\{\delta\}=(\delta_X, \delta_Y, \delta_Z)^T$, respectively. Center of cracking and yield surfaces are expressed as $\{{}_CP^c\}=({}_CQ^c{}_X, {}_CQ^c{}_Y, {}_CN^c)^T$ and $\{{}_CP^y\}=({}_CQ^y{}_X, {}_CQ^y{}_Y, {}_CN^y)^T$, which initial values are $\{{}_CP^c\}=\{{}_CP^y\}=(0, 0, {}_CN)^T$, respectively. The one-axial restoring force models shown in Figure 1 were expressed when $N={}_CN$.

Hardening rule

The yield and cracking surfaces of F-model and S-model obey mixed hardening rule that consist of isotropic hardening rule and Prager's kinematic hardening rule [7]. These surfaces translate and expand according to the mixed hardening rule. Translation and expansion of the yield and cracking surfaces are calculated in the same way. Figure 4(a) shows bound expressing cracking condition in one-axial case, which the range is $2{}_mQ^c{}_X$ and its center is ${}_CQ^c{}_X$. When force increment dQ_X is given at a point A, the bound expressing cracking condition widens $dQ_X/2$ and the center translates $dQ_X/2$. This rule is extended to tri-axial case as shown in Figure 4(b). Then the following relationships are given, where $\{{}_CP^c\}$ and h^c are center and expanding ratio of the cracking surface, which details of leading equation were shown by Nishimura and Takiguchi [6].

$$dh^c = \frac{\{\partial F^c/\partial P\}^T \{d\,{}_CP^c\}}{\{\partial F^c/\partial P\}^T (\{P\}-\{{}_CP^c\})} \tag{5}$$

$$\{d\,{}_CP^c\} = \frac{\{\partial F^c/\partial P\}\cdot\{\partial F^c/\partial P\}^T}{2\cdot\{\partial F^c/\partial P\}^T\cdot\{\partial F^c/\partial P\}}\cdot\{dP\} \tag{6}$$

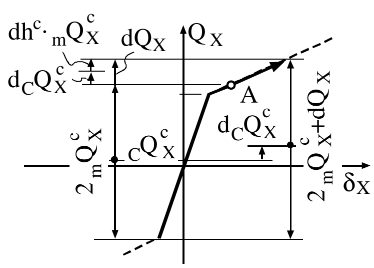

(a) One-axis

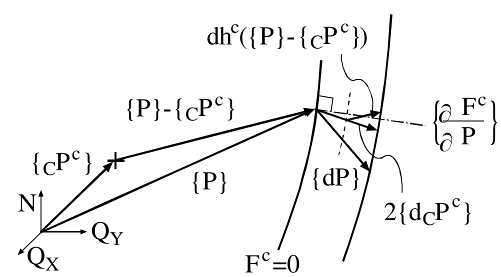

(b) Multi-axes

Figure 4 Mixed hardening

Modeling of behavior on unloading stage

Corn in deformation space

Figure 5(a) shows Q_X-δ_X and δ_X-δ_Z relationship curves of a R/C column under a constant axial force. It can be said that force-deformation behaviors on loading stage are analogous to the theory of plasticity [5]. However it is difficult to describe a behavior on unloading stage by using the theory of plasticity, which behaviors that axial deformation directs toward compressive side on unloading stage as shown in Figure 5(a) can be often seen on R/C structures. Nishimura and Takiguchi presented elastic rigidity that considered interaction between lateral and vertical components and loading surface to describe the behavior on unloading stage [6]. The behavior on unloading stage was modeled as shown in Figure 5(b) that the deformation directed to point T. This modeling method was extended to tri-axial space shown in Figure 5(c), which the deformation point moves on a cone under a constant axial force. The point T shown in Figure 5(c) is expressed as $\{{}_T\delta\}=({}_T\delta_X, {}_T\delta_Y, {}_T\delta_Z)^T$. The cone is expressed as follows, where r_X, r_Y, and r_Z are axis length of ellipse in X and Y direction and height of cone, respectively.

$$f_{cone} = (\delta_X - {}_T\delta_X)^2/{r_X}^2 + (\delta_Y - {}_T\delta_Y)^2/{r_Y}^2 - (\delta_Z - {}_T\delta_Z)^2/{r_Z}^2 = 0 \tag{7}$$

r_Y is assumed to be equal to r_X in this paper. r_X, and r_Z can be given by {δ} and {$_T$δ}. In this paper, translation of the corn is assumed as follows, where [K^e] is elastic rigidity.

$$\{d_T\delta\} = [K^e]\cdot(0 \quad 0 \quad dN)^T \tag{8}$$

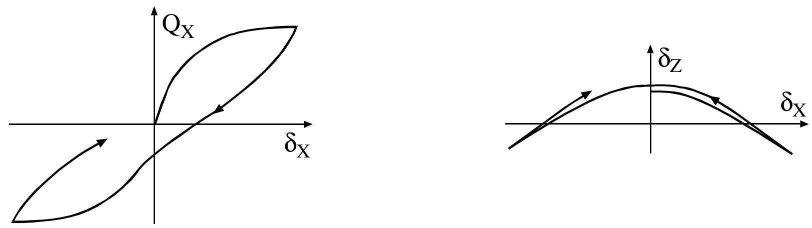

(a) Restoring force characteristics of a R/C column under a constant axial force

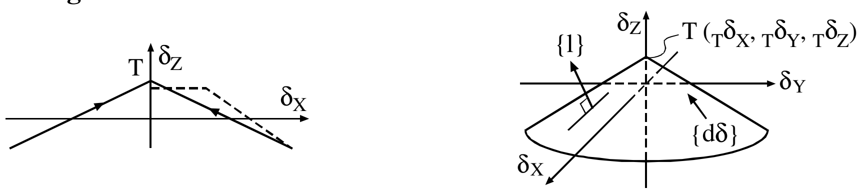

(b) Modeling of deformation **(c) Modeling in tri-axial case**

Figure 5 Modeling of behavior on unloading stage

Elastic rigidity

Elastic rigidity was assumed to be able to express the behavior that the deformation increment vector {dδ} lays on the cone under a constant axial force as follows [6].

$$[K^e] = \begin{bmatrix} \alpha_X^e \cdot K_X + w_X{}^2 \cdot \alpha_Z^e \cdot K_Z & 0 & -w_X \cdot \alpha_Z^e \cdot K_Z \\ & \alpha_Y^e \cdot K_Y + w_Y{}^2 \cdot \alpha_Z^e \cdot K_Z & -w_Y \cdot \alpha_Z^e \cdot K_Z \\ sym. & & \alpha_Z^e \cdot K_Z \end{bmatrix}, \tag{9}$$

where $w_X = \dfrac{(\delta_X - {}_T\delta_X)\cdot(\delta_Z - {}_T\delta_Z)}{(\delta_X - {}_T\delta_X)^2 + k_r{}^2\cdot(\delta_Y - {}_T\delta_Y)^2}$, $w_Y = \dfrac{k_r{}^2\cdot(\delta_Y - {}_T\delta_Y)\cdot(\delta_Z - {}_T\delta_Z)}{(\delta_X - {}_T\delta_X)^2 + k_r{}^2\cdot(\delta_Y - {}_T\delta_Y)^2}$, $k_r = \dfrac{r_X}{r_Y} = 1.0$. (10)

Loading surface

The loading surface is corresponded to corner of the parallelogram loop of F-model. The loading surface and its center is expressed as F^l=0 and {$_CP^l$}=($_CQ_X{}^l$, $_CQ_Y{}^l$, $_CN^l$). As shown in Figure 6, loading surfaces are assumed on a virtual plane and Z-axis those are expressed as $_bF^l$=0 and $_ZF^l$=0, respectively. $_bF^l$=0 is represented as an ellipse, where circle is used in this model, and $_ZF^l$=0 decides the range of Z component of a force point. Those conditions are expressed as follows.

$${}_bF^l = \left(\frac{{}_bQ_X - {}_{Cb}Q_X^l}{{}_mQ_X^l}\right)^2 + \left(\frac{{}_bQ_Y - {}_{Cb}Q_Y^l}{{}_mQ_Y^l}\right)^2 - 1 \quad \text{[On virtual plane]} \tag{11}$$

$${}_ZF^l = \left(\frac{N - {}_CN^l}{{}_mN^l}\right)^2 - 1 \quad \text{[On Z axis]} \tag{12}$$

$\{_bP\}=(_bQ_X,\ _bQ_Y)^T$ and $\{_{Cb}P^l\}=(_{Cb}Q^l_X,\ _{Cb}Q^l_Y)^T$ are a force point and a center of loading surface on virtual plane. Initial values in Equation (11) and (12) are given as $_{Cb}Q^l_X={}_{Cb}Q^l_Y=0$, $_CN^l={}_CN$, $_mQ^l_X={}_mQ^c_X$, $_mQ^l_Y={}_mQ^c_Y$, and $_mN^l={}_mN^c$. Judgments of relationship between a force point and loading surface in tri-axial space are assumed as follows.

$$F^l(P)=0,\ \text{if}\ {}_bF^l({}_bP)=0\ \text{or}\ {}_ZF^l(N)=0. \tag{13}$$

$$F^l(P)<0,\ \text{if}\ {}_bF^l({}_bP)<0\ \text{and}\ {}_ZF^l(N)<0. \tag{14}$$

A plastic flow associated with loading surface is expressed as follows by using the flow rule.

$$\{d\delta^l\}=d\lambda^l\left\{\frac{\partial F^l}{\partial P}\right\} \tag{15}$$

$\{\partial F^l/\partial P\}$ is assumed to lie in direction along the corn shown in Figure 5(c) when $_bF^l(_bP)=0$, and to lie in direction along Z-axis when $_ZF^l(N)=0$. Those are expressed as follows, where w_X and w_Y are equal to those in Equation (10).

$$\left\{\frac{\partial F^l}{\partial P}\right\}=\left(\frac{\partial_b F^l}{\partial_b Q_X},\frac{\partial_b F^l}{\partial_b Q_Y},w_X\cdot\frac{\partial_b F^l}{\partial_b Q_X}+w_Y\cdot\frac{\partial_b F^l}{\partial_b Q_Y}\right)^T\ \text{when}\ {}_bF^l({}_bP)=0. \tag{16}$$

$$\left\{\frac{\partial F^l}{\partial P}\right\}=\left(0,0,\frac{\partial_Z F^l}{\partial N}\right)^T\ \text{when}\ {}_ZF^l(N)=0. \tag{17}$$

The loading surface obeys Prager's kinematic hardening rule, and the following equation can be given.

$$\{d\,{}_CP^l\}=\frac{\{\partial F^l/\partial P\}\cdot\{\partial F^l/\partial P\}^T}{\{\partial F^l/\partial P\}^T\cdot\{\partial F^l/\partial P\}}\cdot\{dP\} \tag{18}$$

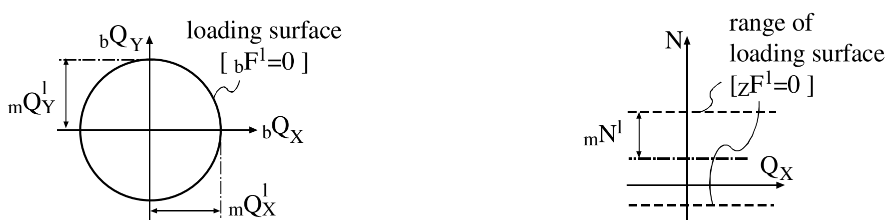

(a) On virtual plan **(b) On Z-axis**

Figure 6 Loading surface

Transformation of force point

A force point $\{P\}$ in tri-axial force space is transformed to a point $\{_bP\}$ on the virtual plane. $\{P\}$ is projected on the virtual plane, and coefficient of influence of axial force modifies projected vector as follows, where $\{P'\}=(_bQ_X,\ _bQ_Y,\ 0)^T$ and k_n is the coefficient.

$$\{dP'\}=k_n\cdot\left[[I]-\frac{\{l\}\cdot\{n\}^T}{\{n\}^T\cdot\{l\}}\right]\cdot\{dP\} \tag{19}$$

[I] is unit matrix, {l} is normal vector of the corn shown in Figure 5(c), and {n} is a unit vector lies in positive direction of Z-axis. A center of loading surface $\{_CP^l\}$ is also transformed to a point on virtual plane in the same way. In this paper, k_n is assumed to consider difference in cracking strength under different axial force as follows.

$$k_n = 1 - \left\{ (N - {_C}N^c) / {_m}N^c \right\}^2 \quad \text{[F-model]} \tag{20}$$

$$k_n = \sqrt{1 - \left\{ N - {_C}N^c / {_m}N^c \right\}^2} \quad \text{[S-model]} \tag{21}$$

Top of corn

As shown in Figure 7, a top of the corn shown in Figure 5(c) is made smooth by parabola in small range to have no corner because the corner make calculation difficult. In this paper, the range of parabola is ${_m}\delta^y{_X}/50$ in X-direction. ${_m}\delta^y{_X}$, which is shown in Table 2, is explain later. The range in Y- directions are calculated the same as X-direction.

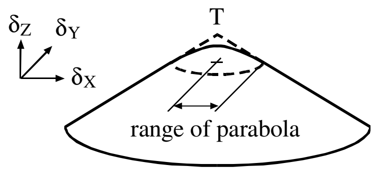

Figure 7 Top of corn

Force-deformation relationship

Force and deformation increment relationship can be written as follows.

$$\{dP\} = [K] \cdot \{d\delta\} \tag{22}$$

In this paper, elastic state is named E-state, and elastic-plastic state associated with cracking surface is named EC-state. Elastic-plastic state associated with loading, cracking and yield surfaces is named ELCY-state in the same rule. According to the total number of surfaces, F-model has eight states, and S-model has four states. [K] shown in Equation (22) is rigidity on each state. [K] is equal to $[K^e]$ in E-state. Rigidities in the other state can be obtained based on the theory of elasticity and plasticity [8], and rigidity in ECY-state can be obtained as follows for example.

$$\left[K^{ecy}\right] = \left[[K^e]^{-1} + \frac{\{\partial F^c / \partial P\} \cdot \{\partial F^c / \partial P\}^T}{\{\partial F^c / \partial P\}^T \cdot [k^c] \cdot \{\partial F^c / \partial P\}} + \frac{\{\partial F^y / \partial P\} \cdot \{\partial F^y / \partial P\}^T}{\{\partial F^y / \partial P\}^T \cdot [k^y] \cdot \{\partial F^y / \partial P\}} \right]^{-1} \tag{23}$$

$[k^l]$, $[k^c]$ and $[k^y]$ are plastic rigidities associated with loading, cracking and yield surfaces, respectively. Those are written as follows.

$$\left[k^l\right] = \begin{bmatrix} \gamma_X^l K_X & 0 & 0 \\ 0 & \gamma_Y^l K_Y & 0 \\ 0 & 0 & \gamma_Z^l K_Z \end{bmatrix}, \left[k^c\right] = \begin{bmatrix} \gamma_X^c K_X & 0 & 0 \\ 0 & \gamma_Y^c K_Y & 0 \\ 0 & 0 & \gamma_Z^c K_Z \end{bmatrix}, \left[k^y\right] = \begin{bmatrix} \gamma_X^y K_X & 0 & 0 \\ 0 & \gamma_Y^y K_Y & 0 \\ 0 & 0 & \gamma_Z^y K_Z \end{bmatrix} \tag{24}$$

These rigidities are given by one-axial restoring force model. Figure 8 shows plastic rigidities on X-axis of F-model. The rigidities on the other axis and the rigidities of S-model can be obtained in the same way. γ_X^l, γ_X^c and γ_X^y of F-model and S-model are expressed as follows.

$$\gamma_X^l = \frac{\alpha_X^e \cdot \alpha_X^{el}}{\alpha_X^e - \alpha_X^{el}},\ \gamma_X^c = \frac{\alpha_X^{el} \cdot \beta_X}{\alpha_X^{el} - \beta_X},\ \gamma_X^y = \frac{\beta_X \cdot p_X}{\beta_X - p_X} \quad \text{[F-model]} \tag{25}$$

$$\gamma_X^c = \frac{\alpha_X^e \cdot \beta_X}{\alpha_X^e - \beta_X},\ \gamma_X^y = \frac{\beta_X \cdot p_X}{\beta_X - p_X} \quad \text{[S-model]} \tag{26}$$

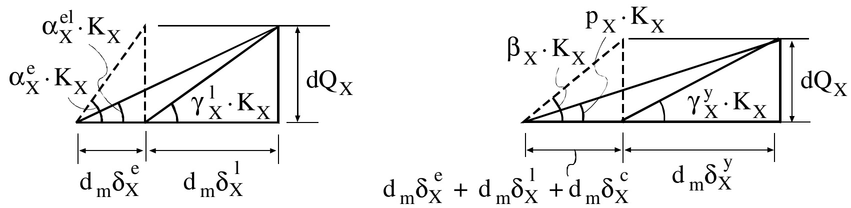

EL state ELCY state

Figure 8 Plastic rigidity of F-model

Rigidity degradation

Rigidity degradation of restoring force model presented by Nishimura and Takiguchi [5] is modified in this paper. This paragraph shows rigidity of X-axis, and rigidities of Y and Z axes can be calculated as those of X-axis. As shown in Figure 9, α^c_X of F-model and S-model are given as follows.

$$\alpha_X^c = {}_mQ_X^c / (K_X \cdot {}_m\delta_X^c) \ \text{ where } d\,{}_mQ_X^c = dh^c \cdot {}_mQ_X^c \tag{27}$$

Increments of ${}_m\delta^c_X$ are assumed as shown in Table 1. Coefficients shown in Table 1, which are γ^{ec}_X and γ^{ecy}_X for example, are given in the same way shown in Figure 8 by substituting $d_mQ^c_X$ for dQ_X.

Table 1 Increments of ${}_m\delta^c_X$

	F-model	S-model
EC-state	$d\,{}_m\delta_X^c = d\,{}_mQ_X^c / (\gamma_X^{ec} \cdot K_X)$	$d\,{}_m\delta_X^c = d\,{}_mQ_X^c / (\beta_X \cdot K_X)$
EY-state	$d\,{}_m\delta_X^c = d\,{}_mQ_X^c / (\gamma_X^{ey} \cdot K_X)$	$d\,{}_m\delta_X^c = d\,{}_mQ_X^c / (\gamma_X^{ey} \cdot K_X)$
ELC-state	$d\,{}_m\delta_X^c = d\,{}_mQ_X^c / (\beta_X \cdot K_X)$	-
ELY-state	$d\,{}_m\delta_X^c = d\,{}_mQ_X^c / (\gamma_X^{ely} \cdot K_X)$	-
ECY-state	$d\,{}_m\delta_X^c = d\,{}_mQ_X^c / (\gamma_X^{ecy} \cdot K_X)$	$d\,{}_m\delta_X^c = d\,{}_mQ_X^c / (p_X \cdot K_X)$
ELCY-state	$d\,{}_m\delta_X^c = d\,{}_mQ_X^c / (p_X \cdot K_X)$	-

Elastic rigidity degradation of F-model is assumed as shown in Figure 10. The elastic rigidity before yielding is degraded as a point direct to the point of maximum deformation experienced. The rigidity after yielding is degraded according to ratio between maximum yield deformation ${}_m\delta^y_X$ and initial yield deformation ${}_Y\delta_X$ [9]. The following equation is given to express this rule.

$$\alpha_X^e \cdot K_X = \alpha_X \cdot \left(\frac{{}_m\delta_X^y}{{}_Y\delta_X} \right)^{\gamma} \cdot K_X \tag{28}$$

α_X is the lower value between α^c_X and ${}_{im}Q^y_X/{}_Y\delta_X$, where ${}_{im}Q^y_X$ is initial value of ${}_mQ^y_X$. An increment of ${}_m\delta^y_X$ is assumed as shown in Table 2. ${}_C\alpha_X^{el}$ of F-model, which ${}_C\alpha_X^{el}K_X$ is rigidity of EL-state when N=${}_C$N, can be calculated with α_X^e and α_X^c as follows.

$$ {}_C\alpha_X^{el} = ({}_mQ_X^c - {}_mQ_X^l) \big/ ({}_mQ_X^c \big/ \alpha_X^c - {}_mQ_X^l \big/ \alpha_X^e) \tag{29} $$

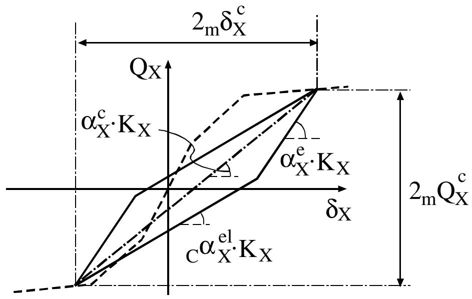

Figure 9 Rigidity of loop

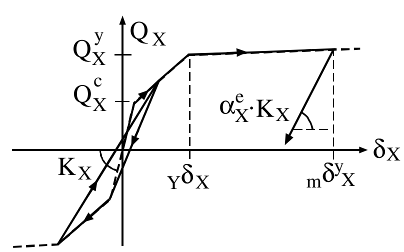

Figure 10 Elastic rigidity degradation of F-model

Table 2 An Increment of ${}_m\delta^y_X$ of F-model

EY-state	$d\,{}_m\delta_X^y = d\,{}_mQ_X^y \big/ (\gamma_X^{ey} \cdot K_X)$
ELY-state	$d\,{}_m\delta_X^y = d\,{}_mQ_X^y \big/ (\gamma_X^{ely} \cdot K_X)$
ECY-state	$d\,{}_m\delta_X^y = d\,{}_mQ_X^y \big/ (\gamma_X^{ecy} \cdot K_X)$
ELCY-state	$d\,{}_m\delta_X^y = d\,{}_mQ_X^y \big/ (p_X \cdot K_X)$

Regarding one-axial force-deformation relationship under a constant axial force that is equal to ${}_C$N, a point directs toward a point of the maximum deformation experienced if α^e_X, ${}_C\alpha^{el}_X$ and α^c_X are used. However, if axial force is different from ${}_C$N, a point may not direct toward the point of the maximum deformation experienced because of difference in lateral strength depending on axial force as shown in Figure 11. The model presented by Nishimura and Takiguchi [6] used ${}_C\alpha^{el}_X$ for α^{el}_X of F-model and α^c_X α^e_X of S-model in every axial force. The restoring force models in this paper are modified this problem. α^{el}_X of F-model and α^e_X of S-model are assumed as axial force effects can be considered, as follows.

$\alpha_X^{el} = k_n \cdot {}_C\alpha_X^{el}$ for F-model, where k_n is equal to Equation (20). (30)

$\alpha_X^e = k_n \cdot \alpha_X^c$ for S-model, where k_n is equal to Equation (21). (31)

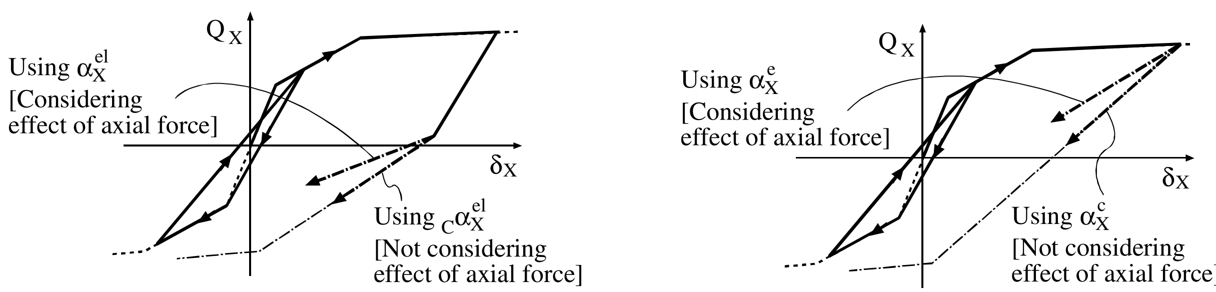

(a) F-model **(b) S-model**

Figure 11 Effect of axial force

EARTHQUAKE RESPONSE ANALYSIS

Numerical program

Earthquake responses of R/C structures were examined with the one-mass-system and the two types of restoring force model those were F-model and S-model. Newmark method [β=1/4] was used for the response analysis, and three earthquake ground motions those were Chi Chi 1999, Kobe 1995, and El Centro 1940 were inputted. Constants of the F-model and the S-model were decided based on experimental results of R/C columns [5] and R/C box wall structures [10], as shown in Table 3. Coefficient of damping was calculated with damping factor and instant stiffness of the system on each step. Parameters of the analysis were natural period ranged from 0.1 to 0.6sec and types of analysis those were tri-axial and lateral bi-axial analyses. The natural period corresponds to initial elastic stiffness of the model. The restoring force model of bi-axial analysis is the same to the model of tri-axial analysis except for having no Z-directional components.

A total plastic deformation can be given as shown in Figure 12. A total plastic deformation ratio η in one-axial case can be estimated by Δh, p, β, and ξ. The equation shown in Figure 12 was adopted in tri-axial and bi-axial analyses. In this paper, earthquake response analyses were carried out as η got to 20.0 in F-model and 0.5 in S-model those were decided based on the past experimental study [5][10]. Δh corresponded to η was calculated, and then analyses were made by controlling yield strength as Δh got to the calculated values.

Table 3 Constants of the system

	F-model	S-model
β_X (=β_Y=β_Z)	0.27	0.21
p_X (=p_Y=p_Z)	0.001	0.001
Axial force ratio	0.25	0.1
Ratio of yield strength to cracking strength	2.2	3.3
Axial yield strength ratio of tension to compression	0.25	0.25
Axial cracking strength ratio of tension to compression	0.1	0.1
γ shown in Equation (28)	-0.5	-
Damping factor	0.02	0.05
Ratio of vertical natural period to lateral natural period	0.3	0.3

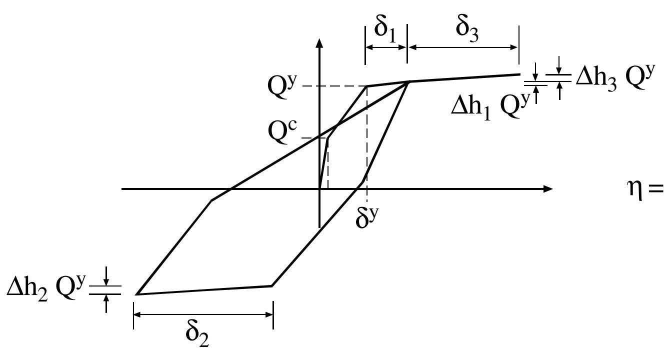

$$\eta = \frac{\text{Total plastic deformation } (=\delta_1+\delta_2+\delta_3)}{\text{Yield deformation } (=\delta^y)} = \frac{\Delta h/p}{\xi + (1-\xi)/\beta},$$

$$\text{where } \Delta h = \Delta h_1+\Delta h_2+\Delta h_3 \text{ and } \xi = \frac{Q^c}{Q^y}$$

Figure 12 Total plastic deformation

Numerical results

Figure 13 shows responses in case of inputting Kobe ground motion. Initial natural periods of the system are 0.2sec for F-model and 0.1sec for S-model. Mg in Figure 13 is gravitation acting on the system. UD-axis takes compressive side as positive direction. As shown in Figure 13, the restoring force model shown in this paper could represent behaviors on unloading stage, which UD-directional deformation direct to compressive side.

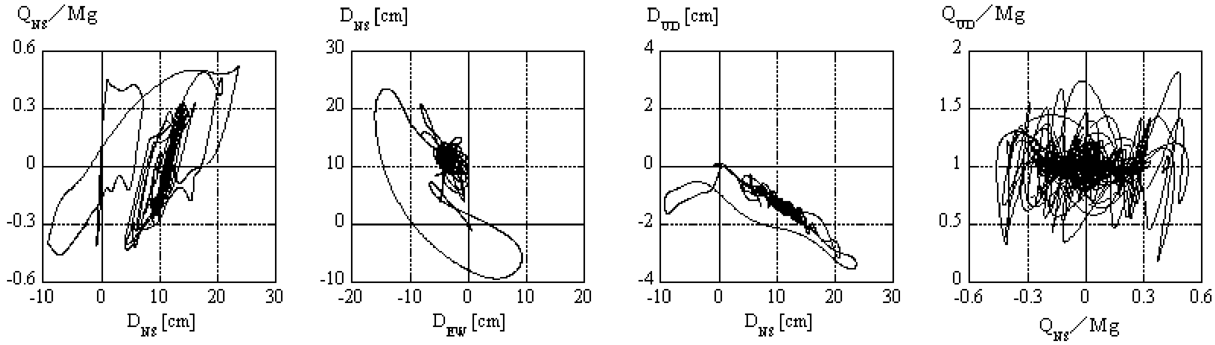

(a) F-model with 0.2sec initial natural period

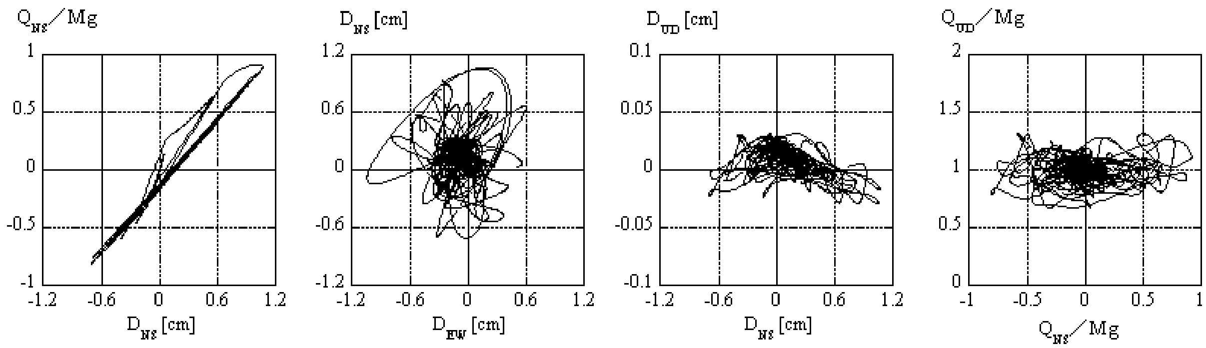

(a) S-model with 0.1sec initial natural period

Figure 13 Reponses inputted Kobe ground motion

Figure 14 shows numerical results when Chi Chi, Kobe, and El Centro ground motions were inputted. Circle and diamond marks represent the results of F-model and S-model, respectively. White and black marks represent tri-axial and bi-axial analyses, respectively. D, A, A_V, V_E, and T express maximum lateral deformation response, maximum lateral absolute acceleration response, maximum vertical absolute acceleration response, equivalent velocity of total energy input [11], and initial natural period of the system, respectively. D is equal to a square root of sum of δ_{NS}^2 and δ_{EW}^2. A is calculated in the same way as D. V_E can be given as follows, where E and M are total energy input and mass of the system, respectively.

$$V_E = \sqrt{2E/M} \tag{32}$$

D-T, A-T, and V_E-T relationships of tri-axial analysis almost agreed with the relationships of bi-axial analysis as shown in Figure 14(a) to (c). These results indicate possibility that it is enough to consider lateral two directional input of earthquake motion when we estimate lateral external force and maximum deformation in seismic design. It is important to know the maximum deformation to judge whether non-structural claddings of buildings can follow the deformation.

The maximum and the minimum vertical absolute acceleration responses are both plotted in Figure 14(d). As shown in this figure, absolute values of the responses of positive and negative side were almost equal. The largest values were about 940 cm/sec^2 on the F-model of 0.3sec period inputted Kobe ground motion, and about 1,090 cm/sec^2 on the S-model of 0.5sec period inputted Kobe ground motion. It can be said that

A_V were obtained in the range of 300 to 1,100 cm/sec^2. Although these results may not be serious from the viewpoint of collapse of structures, it is necessary to consider these results from the viewpoint of influence on inside of buildings.

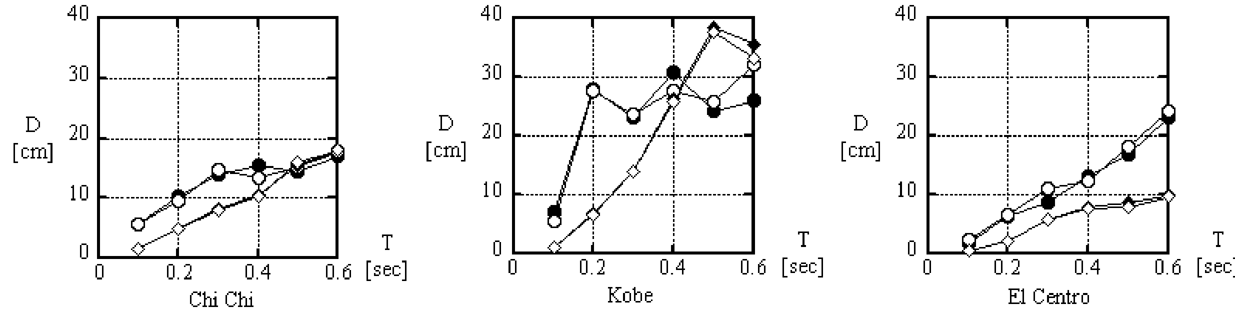

(a) Maximum lateral deformation responses

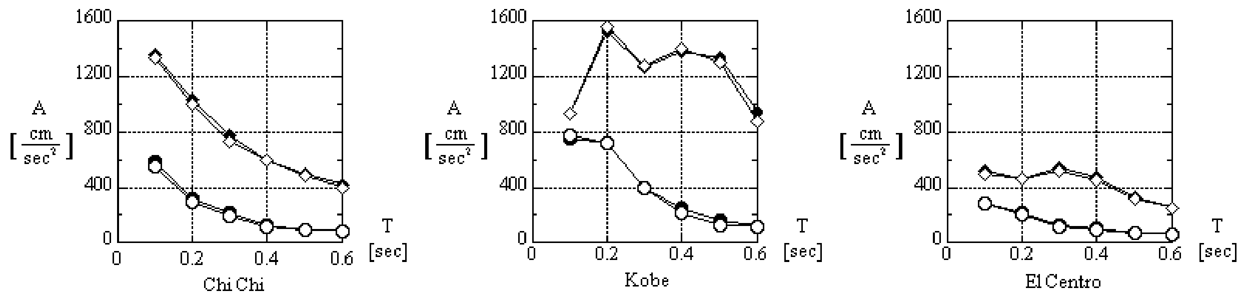

(b) Maximum lateral acceleration responses

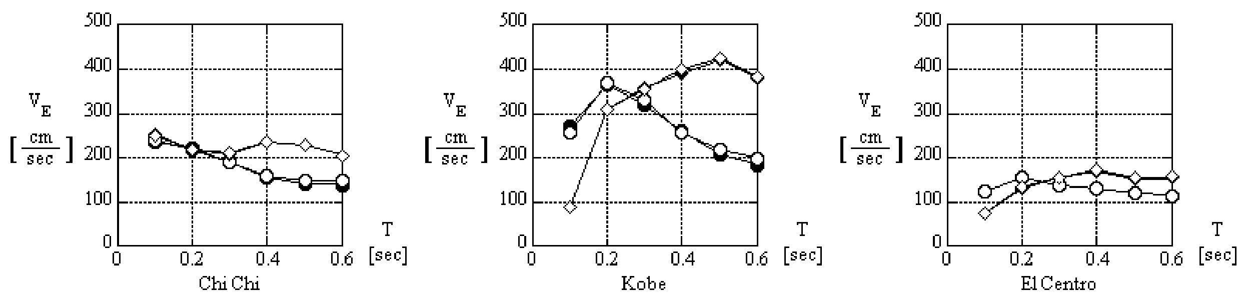

(c) Equivalent velocity of total energy input

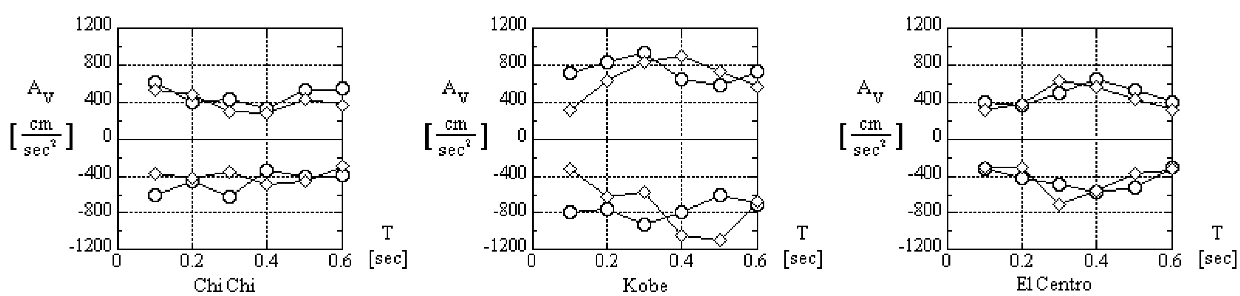

(d) Maximum vertical absolute acceleration responses

Figure 14 Earthquake responses

Evaluation of total energy input

An evaluation of the total energy input of tri-axial non-linear earthquake response was examined with a result of elastic response analysis, which damping factor is 0.1sec [11]. Figure 15 shows V_E-T relationships where a solid curve express a result of tri-axial elastic response analysis, which damping factor is 0.1sec. Circle and diamond marks are represented the results of F-model and S-model, respectively. The results are plotted by averaged periods those were averages of two periods associated with initial elastic stiffness and last value of $\alpha^c{}_X$ shown in Figure 1. V_E of F-model and S-model show good agreement with the elastic analysis results. There are some differences between the results of elastic analysis and non-linear analysis in the range of longer period, however those are safety side and those differences aren't large. Therefore, it can be said a result of tri-axial elastic response analysis with 0.1 damping factor has possibility to be able to evaluate total energy input of tri-axial non-linear earthquake response of R/C structures by using the averaged periods.

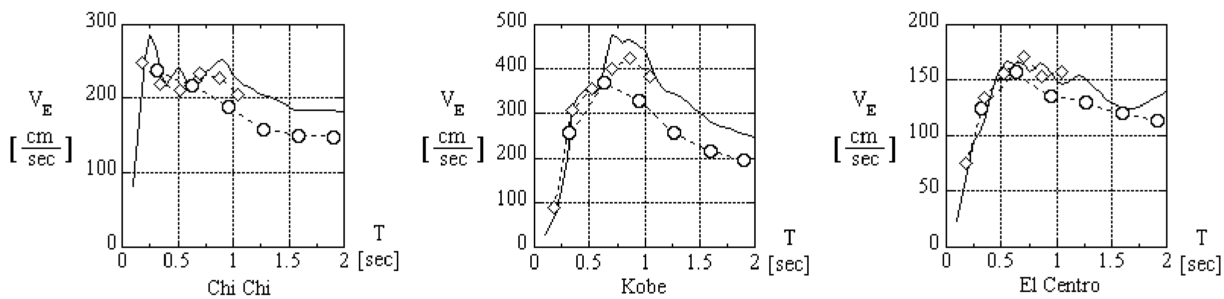

Figure 15 Evaluation of total energy input

CONCLUSIONS

Tri-axial multi-linear restoring force models of R/C structures, which were based on the theory of plasticity, were shown in this paper. The model presented by Nishimura and Takiguchi in 2003 [6] were modified, and flexural and shear types of R/C structure were modeled. The flexural type can be seen in rigid frame structures that have large area in hysterisis loop, and the shear type can be seen in R/C box wall structures that have small area in the loop. Tri-axial non-linear earthquake responses of R/C structures were examined with one-mass system and these two types of restoring force model. Parameters of the analyses were natural period ranged from 0.1 to 0.6sec and types of analysis those were tri-axial and bi-axial analyses. The natural period corresponds to initial elastic stiffness of the model. Chi Chi, Kobe, and El Centro earthquakes were employed for input data. As a result, the following conclusions were found.

1) The tri-axial multi-linear restoring force model of R/C structures shown in this paper could describe behaviors that axial deformation directed toward compressive side on unloading stage, which representation of these behaviors were one of the problems of restoring force models based on the theory of plasticity.
2) Maximum lateral deformation response, maximum lateral absolute acceleration response, and total energy input of tri-axial analysis were almost equal to the responses of lateral bi-axial analysis. These results indicate possibility that it is enough to consider two directional input of earthquake motion to estimate lateral external force and maximum deformation in seismic design.
3) Maximum vertical absolute acceleration responses of tri-axial analyses were obtained in the range of 300 to 1,100 cm/sec^2. Although these results may not be serious from the viewpoint of collapse of structures, it is necessary to consider these results from the viewpoint of influence on inside of buildings.

4) Total energy input of tri-axial elastic response analysis with 0.1 damping factor showed good agreement with result of tri-axial non-linear response at an averaged period that was an average of two periods associated with initial elastic stiffness and last stiffness that connected a point of maximum deformation experienced and a point of minimum deformation experienced diagonally. It can be said that the result of tri-axial elastic response analysis with 0.1 damping factor has possibility to be able to evaluate the total energy input of tri-axial non-linear earthquake response of R/C structures by using the averaged periods.

REFERENCES

1. Takizawa H, Aoyama H. “Biaxial effects in modeling earthquake response of R/C structures.” Earthquake Engineering and Structural Dynamics, 1976, Vol.4: 523-552.
2. Yoshimura M, Aoyama H, Kawamura M. “Analysis of reinforced concrete structure subjected to two-dimensional forces, Part1: Analysis of RC columns subjected to bi-axial bending.” Journal of Structural and Construction Engineering, Architectural Institute of Japan, 1985, No.298: 31-41. (in Japanese)
3. Isozaki Y, Fukuzawa E, Takahashi M. “Elasto-plastic earthquake response analysis of reinforced concrete space frame in consideration of biaxial bending moments and varying axial forces on columns, Part 1 Analytical method.” Journal of Structural and Construction Engineering, Architectural Institute of Japan, 1992, No.441: 73-83. (in Japanese)
4. Takiguchi K, Gao Z. “Tri-axial non-linear restoring force model of R/C structure using the theory of plasticity.” Proceedings of 12th World Conference on Earthquake Engineering, Auckland, New Zealand, 2000. Paper ID 0693.
5. Takiguchi K, Nishimura K, Hirai K. “Experimental study on two-dimensional restoring force characteristics of R/C columns under varying axial force.” Journal of Structural and Construction Engineering, Architectural Institute of Japan, 2001, No.539: 111-118. (in Japanese).
6. Nishimura K, Takighchi K. “Tri-Axial Non-Linear Restoring Force Model of R/C Structures by Using an Analogy to the Plastic Theory.” Journal of Structural and Construction Engineering, Architectural Institute of Japan, 2003, No.566: 113-120. (in Japanese).
7. Shield R.T, Ziegler H. “On Prager's Hardening Rule.” Zeitschrift fur angewandte Mathematik und Physik, 1958, Vol.9a: 260-276
8. Chen, W.F. “Constitutive equation for engineering materials.” Amsterdam, Holland: Elsevier Science Ltd., 1994.
9. Akiyama H. "Earthquake-Resistant Design Method for Buildings Based on Energy Balance," Tokyo, Japan: Gihodo Shuppan Co.,Ltd., 1999. (in Japanese).
10. Torita H, Nishikawa T, Saito H, Ishikawa Y, and Kitada Y. “Study on Restoring Force Characteristics of a RC Box Wall Subjected to Diagonal Horizontal Force.” Summaries of Technical Papers of Annual Meeting AIJ, 1998, C-2: 865-866. (in Japanese).
11. Akiyama H. "Earthquake-Resistant Limit-State Design for Buildings," Tokyo, Japan: University of Tokyo Press, 1985.